Blading of Conformal Electron-Transport Layers in p–i–n Perovskite Solar Cells

Md Aslam Uddin, Prem Jyoti Singh Rana, Zhenyi Ni, Xuezeng Dai, Zhenhua Yu, Zhifang Shi, Haoyang Jiao, and Jinsong Huang*

Perovskite solar cells (PSCs) are promising to reduce the cost of photovoltaic system due to their low-cost raw materials and high-throughput solution process; however, fabrication of all the active layers in perovskite modules using a scalable solution process has not yet been demonstrated. Herein, the fabrication of highly efficient PSCs and modules in ambient conditions is reported, with all layers bladed except the metal electrode, by blading a 36 ± 9 nm-thick electron-transport layer (ETL) on perovskite films with a roughness of ≈ 80 nm. A combination of additives in phenyl-C_{61}-butyric acid methyl ester (PCBM) allows the PCBM to conformally cover the perovskites and still have a good electrical conductivity. Amine-functionalized molecules are added to enhance both the dispersity of PCBM and the affinity to perovskites. A PCBM dopant of 4-(2,3-dihydro-1,3-dimethyl-1*H*-benzimidazol-2-yl)-*N*,*N*-dimethylbenzenamine (N-DMBI) recovers the conductivity loss induced by the small amine molecules. PSCs (0.08 cm²) fabricated by the all-blading process reach an average efficiency of $22.4 \pm 0.5\%$ and a champion efficiency of 23.1% for perovskites with a bandgap of 1.51 eV, with much better stability compared to evaporated ETL PSCs. The all-bladed minimodule (25.03 cm²) shows an aperture efficiency of $\approx 19.3\%$, showing the good uniformity of the bladed ETLs.

1. Introduction

Power conversion efficiency of over 25.5% has recently been reported for metal halide perovskite photovoltaic small-area laboratory cells.[1,2] However, almost all the reported high-efficiency solar cells were fabricated using spin-coating process which cannot be used to fabricate large-area perovskite solar modules. There have been tremendous efforts devoted to deposit perovskite layer using scalable coating methods, such

as blading,[3,4] slot die,[5,6] bar-coating,[7] etc. However nearly all the reported perovskite modules still have a combination of different deposition methods for perovskites and charge-transport layers in a perovskite solar module, despite these layers can in principle be coated by all-solution-processes.[8–10] For p–i–n structure perovskite modules, the hole-transport layer (HTL) such as poly[bis(4-phenyl)(2,5,6-trimethyl-phenyl)amine (PTAA) and perovskite layer are already bladed,[4] while ETLs were still deposited by a high-vacuum process. It will become the rate limiting bottleneck in mass production process, in addition to the extra cost associated with it. Thus, for the commercialization of this rising technology, scalable fabrication of all the functional layers, including HTL, perovskite layer and ETLs is necessary for both sheet-to-sheet and roll-to-roll fabrication to reduce the cost and increase fabrication throughput. There are already several attempts to fabricate perovskite solar cells by all solution process using scalable coating methods.[11–13] However, these studies only resulted in devices with much lower performance than those made of evaporated ETL. For example, few attempts to fabricate PCS with all the bladed layers except evaporation of metal contact delivered a maximum power conversion efficiency (PCE) ranging from 14.9% to 20.3%.[11,12] Other studies reported fully spray-coated PSCs but with relatively lower efficiency ranging from 9% to 12%.[13,14] Slot-die coating reported to print the PCBM layer and other layers on flexible substrates showed much lower efficiency (2.9–11.2%) compared to those of aforementioned techniques.[15,16]

These low-performance PSCs came from the difficulty in coating high-quality ETLs on rough perovskite films. Perovskite films made by solution process are generally rough with a peak-to-valley difference exceeding 80 nm; however, the optimal thickness of fullerene and its derivatives, the most studied electron-transport materials in perovskite solar cells, is generally around 30 nm. Direct blading of PCBM films on perovskite films generally results in noncontinuous and nonconformal coating on perovskites. In addition, the aggregations of PCBM molecules associated with solution deposition methods would make the fiormity even worse. Thus, perovskites can directly contact metal electrodes, which increases nonradiative

M. A. Uddin, P. J. S. Rana, Z. Ni, X. Dai, Z. Yu, Z. Shi, H. Jiao, J. Huang
Department of Applied Physical Sciences
University of North Carolina at Chapel Hill
Chapel Hill, NC 27599, USA
E-mail: jhuang@unc.edu

J. Huang
Department of Chemistry
University of North Carolina at Chapel Hill
Chapel Hill, NC 27599, USA

recombination of charges and accelerates the reaction of metal with perovskites, resulting in inferior device efficiency and stability. This issue cannot be solved by simply increasing thickness of the PCBM layer, because thick PCBM layers have too large resistivity to maintain the device efficiency, despite that the cost of PCBM might not be a limiting factor.

To address these challenges, we designed PCBM and bathocuproine (BCP) ink formulations to completely replace the thermally evaporated C_{60} and BCP layers in p–i–n architecture perovskite solar cells with active area of 0.8 cm^2 and minimodules with aperture area of 25.03 cm^2. We designed a combination of additives to modify both PCBM and BCP layer to enhance the compatibility of inks for blade-coating process. Additives incorporated PCBM (A-PCBM) and BCP inks were found to enhance device and module performance due to the improved surface coverage and electrical conductivity of PCBM. Small-size devices and minimodules fabricated with these inks delivered highest power conversion efficiencies (PCEs) of 23.1% and 19.3%, respectively.

2. ETL Ink Design and Blading

In addition to fullerene and fullerene derivatives,[17–19] other broadly applied ETL materials for high-efficiency perovskite solar cells include TiO$_2$,[20,21] SnO$_2$,[22] ZnO,[23,24] etc. were considered in our study. We chose fullerene derivative as ETL in p–i–n solar cells to avoid the high-temperature annealing process that is generally needed for the oxide ETL materials. PCBM is highly soluble in a number of antisolvents for perovskites, such as common organic solvents of toluene, chlorobenzene, dichlorobenzene.[25] PCBM tends to show aggregation

in its solution.[25] One major issue we identified in fabricating large-area perovskite modules using bladed PCBM is the noncontinuity of the PCBM films. To demonstrate it, we bladed PCBM on perovskites with a composition of FA$_{0.3}$MA$_{0.7}$PbI$_3$ which has the least roughness among all perovskite compositions we have studied as shown by the scanning electron microscopy (SEM) images in **Figure 1**a–c.[9,26] PTAA and FA$_{0.3}$MA$_{0.7}$PbI$_3$ were bladed onto preclean indium tin oxide (ITO) substrate based on our reported methods at room temperature with a control humidity of 30 ± 5%. After blading perovskites, pure PCBM (P-PCBM) solution in chlorobenzene were bladed onto perovskite layer. As shown in Figure 1d–f, PCBM with a typical average thickness of 36 ± 9 nm showed an incomplete surface coverage due to PCBM aggregation as indicated by the appearance of brighter region, where the thickness measurement of PCBM method is shown in Figure S1 in the Supporting Information.

We added small amine molecules—primary (–NH$_2$), secondary (–NHR), and tertiary (–NR$_2$) amines with chemical structures shown in **Figure 2**a and Table S1 (Supporting Information) into PCBM solution to decrease the PCBM aggregation during drying based on a hypothesis that the interaction of these amine molecules with PCBM would prevent the aggregation of PCBM. Before blading the perovskite solution, we tested how amine additive impact PCBM crystallization in the drop-cast PCBM films. As shown in Figure 2a, the drop-cast P-PCBM films had very rough surface. However, when a small amount of 2,7-dibromo-9,9-bis[3-(dimethylamino)propyl]fluorene (DMAPF) with two tertiary amine groups was added into PCBM, the roughness of PCBM films started to decrease. The roughness decreased notably when the molar ratio of DMAPF to PCBM was increased to 0.8%. Considering addition of a large
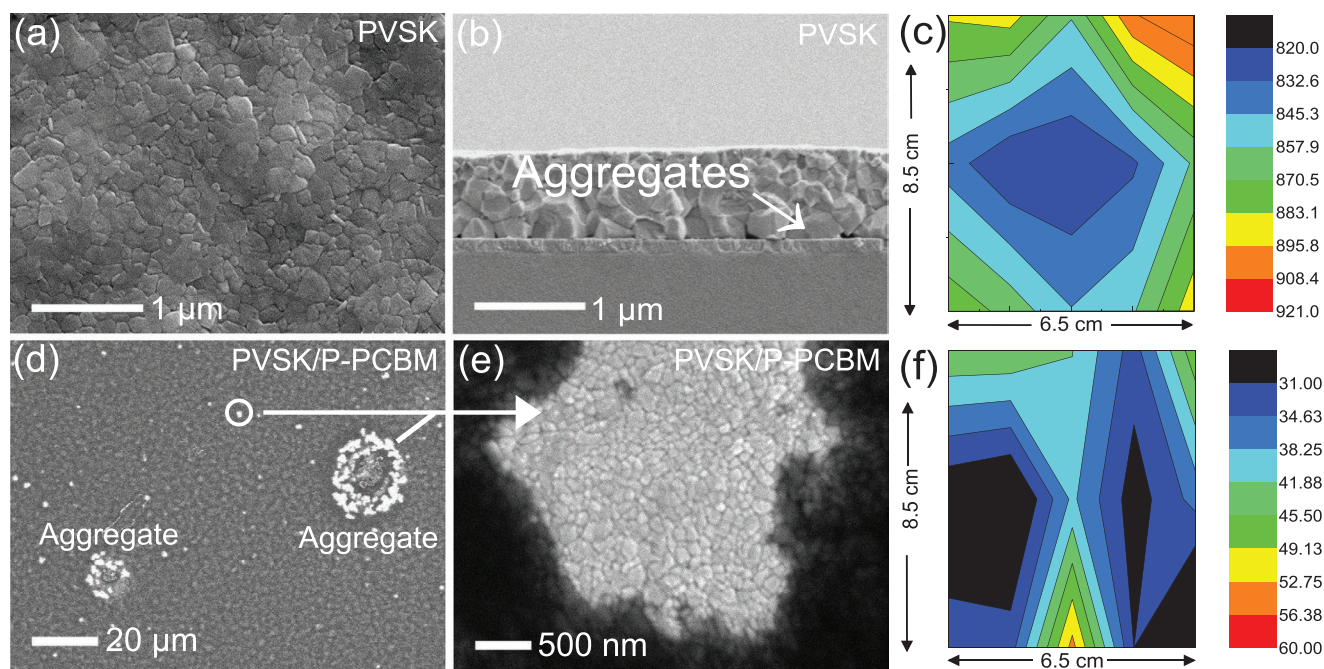

Figure 1. Noncontinuous PCBM films from bladed P-PCBM. a,b) SEM top-view and cross-section image of FA$_{0.3}$MA$_{0.7}$PbI$_3$ perovskite films, respectively, c) thickness of a PVSK film at different locations within an area of 6.5 cm × 8.5 cm, d,e) SEM images of P-PCBM layers onto perovskite layer, and f) thickness of PCBM film at different locations in a module substrate measured using a Dektak XT profiler.
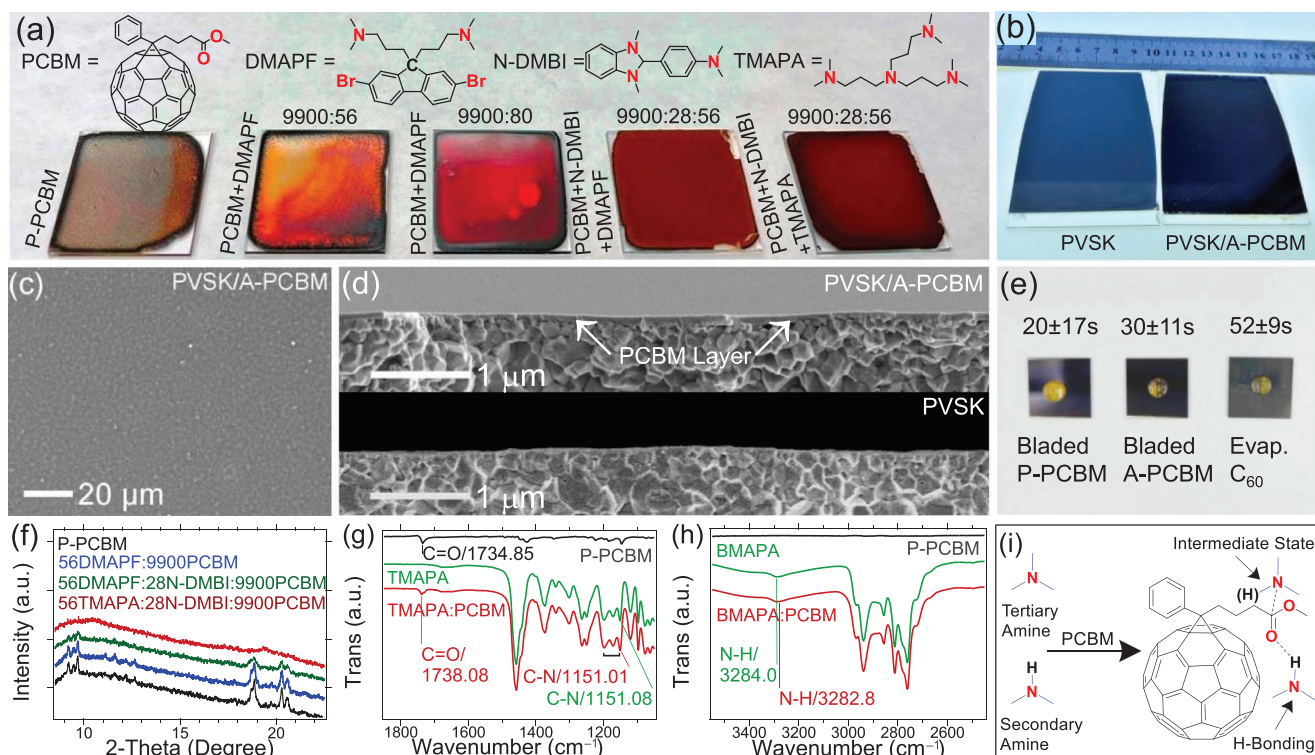
Figure 2. PCBM surface coverage. a) A drop-cast PCBM film and amine-molecule(s)-modified PCBM films, b) photographs of bladed PVSK and DMAPF and N-DMBI incorporated PCBM films with an area of 55.25 cm², c) SEM images of DMAPF and N-DMBI incorporated PCBM, d) comparison of SEM cross-section images of blade-coated PVSK and DMAPF and N-DMBI incorporated PCBM films, e) photograph showing surface coverage tests of bladed P-PCBM, bladed DMAPF and N-DMBI incorporated PCBM, and thermally evaporated C₆₀ films using water droplets, f) XRD patterns of P-PCBM and A-PCBM films fabricated through drop casting of PCBM solutions, g) FTIR spectra of drop-cast P-PCBM, TMAPA, and TMAPA incorporated PCBM films, h) FTIR spectra of drop-cast P-PCBM, BMAPA, and BMAPA incorporated PCBM films, and i) amine additive structures and their interaction with PCBM molecules.

amount of DMAPF molecules may reduce the PCBM conductivity, so a small amount of DMAPF (0.2–0.6%) was replaced by 4-(2,3-dihydro-1,3-dimethyl-1H-benzimidazol-2-yl)-N,N-dimethylbenzenamine (N-DMBI), which behaves dopant in PCBM to enhance its conductivity. A small amount of N-DMBI did not impair the smoothness of PCBM films, because it also contains three tertiary amine groups. As shown in Figure S2 (Supporting Information), we also collected time-resolved photoluminescence lifetime decay data of bladed perovskite films without/with different amine molecules as surface modifiers to see if these amine molecules have the surface passivation effects. It is clearly seen that all the amine molecules passivate the perovskite film surface as lifetime of modified perovskite films is 2–3 times longer than that of bare perovskite films, indicating that amine molecules suppress the nonradiative decay processes. Figure 2b shows photographs of the blade-coated PVSK and PVSK/A-PCBM films with an area of 55.25 cm², showing that the additive makes the PCBM coating to be executed across the large-area films. Figure 2c shows SEM images of DMAPF and N-DMBI additives in PCBM layer eliminated the white spots and PCBM aggregation that were observed for P-PCBM.

We further examine the PCBM coverage and roughness of A-PCBM layer using a combination of characterizations. Cross-section SEM images and SEM images in Figure 2d and Figure S3 (Supporting Information) show a conformal coating of A-PCBM on the perovskite layer with an average PCBM thickness of 43 ± 5 nm. To further check the PCBM coverage, water droplet test was carried out on both thermally evaporated C₆₀ and bladed A-PCBM on perovskite films. As shown in Figure 2e, it took 52 ± 9 and 30 ± 11 s for water to permeate through the evaporated C₆₀ and bladed A-PCBM, respectively to reach the perovskite layers, judging from the color change of PVSK, which indicates the bladed A-PCBM layers have similar coverage as that of thermally evaporated C₆₀ considering the fact that C₆₀ is more hydrophobic than the PCBM. In contrast, the color change of perovskite would only take 20 ± 17 s for P-PCBM bladed on perovskites.

To understand the roles of DMAPF with N-DMBI in dispersing the PCBM molecules and forming PCBM conformal coating, we chose a tertiary and secondary amine molecule—tris-(dimethylaminopropyl)amine (TMAPA) and bis-(dimethylaminopropyl)amine (BMAPA) with the same side chain as of DMAPF for further experiments. We collected XRD patterns of drop-cast P-PCBM, DMAPF incorporated PCBM, DMAPF, and N-DMBI incorporated PCBM, and TMAPA and N-DMBI incorporated PCBM on glass. As shown in Figure 2f, P-PCBM film on glass had good crystallinity with strong XRD peaks, whereas DMAPF and N-DMBI incorporated PCBM and TMAPA and N-DMBI incorporated PCBM showed reduced crystallinity and amorphous nature, respectively, as indicated by the decrease and/or absence of XRD peaks. It proves that

amine additives do prevent aggregation and crystallization of PCBM molecules by dispersing them. Fourier transform infrared (FTIR) spectra is collected to further understand the roles of amine groups in TMAPA and BMAPA in dispersion of PCBM molecules. FTIR spectra is collected using TMAPA and BMAPA in PCBM instead of DMAPF because of the spectral overlap between DMAPF and PCBM. As shown in the FTIR spectra in Figure 2g, the C–O stretching of PCBM showed obvious blueshift from ≈1735 cm^{-1} of P-PCBM to ≈1738 cm^{-1} after mixing them, accompanied with a slightly redshift of N–C stretching in TMAPA, which indicates a strong interaction between them.[27] In addition, amine group may also form hydrogen bond between N–H in BMAPA amine and C–O group PCBM indicated by the redshift of N–H stretching mode from ≈3284 to 3282.7 cm^{-1} as shown in Figure 2h.[27] We speculate these strong interactions, which are illustrated in Figure 2i, should prevent the aggregation of PCBM molecules during drying.

Small solar cells with an active area of 0.08 cm^2 were fabricated with different ETL layers processed with different conditions, and their device performances are summarized in **Figure 3**a.

First, small solar cells with ITO/PTAA/MA$_{0.7}$FA$_{0.3}$PbI$_3$/PCBM/BCP/Cu architecture were fabricated through evaporating BCP and Cu onto bladed A-PCBM layer.[9] The solar cells with bladed A-PCBM and evaporated BCP showed a PCE of 21.6 ± 0.4%, which is comparable to the solar cells with evaporated C$_{60}$/BCP as ETL (21.8 ± 0.4%). When we used both bladed P-PCBM and BCP, the device reproducibility became worse, and the average efficiency reduced to 19.2 ± 2%. This large performance deterioration is attributed to incomplete PCBM coverage. To find out how important the dopant is, we removed N-DMBI from the additive and fabricated devices. Introducing only the amine additive in PCBM still improved the device PCE to 21.3 ± 0.7% which is slightly lower than that of evaporated ETL devices, mainly due to the smaller fill factor (FF) of 0.76 ±0.02 from these devices compared to ≈0.80 ± 0.01 of evaporated ETL devices. The reduced fill factor can be explained by the large resistivity of PCBM with amine additive. Therefore, when N-DMBI as a second additive was introduced in the PCBM solution, FF and average device performance were improved to 0.78 ± 0.03 and 21.8 ± 0.7%, respectively. The same pattern was observed when surface charge extraction capability of P-PCBM and A-PCBM were measured for PVSK/PCBM
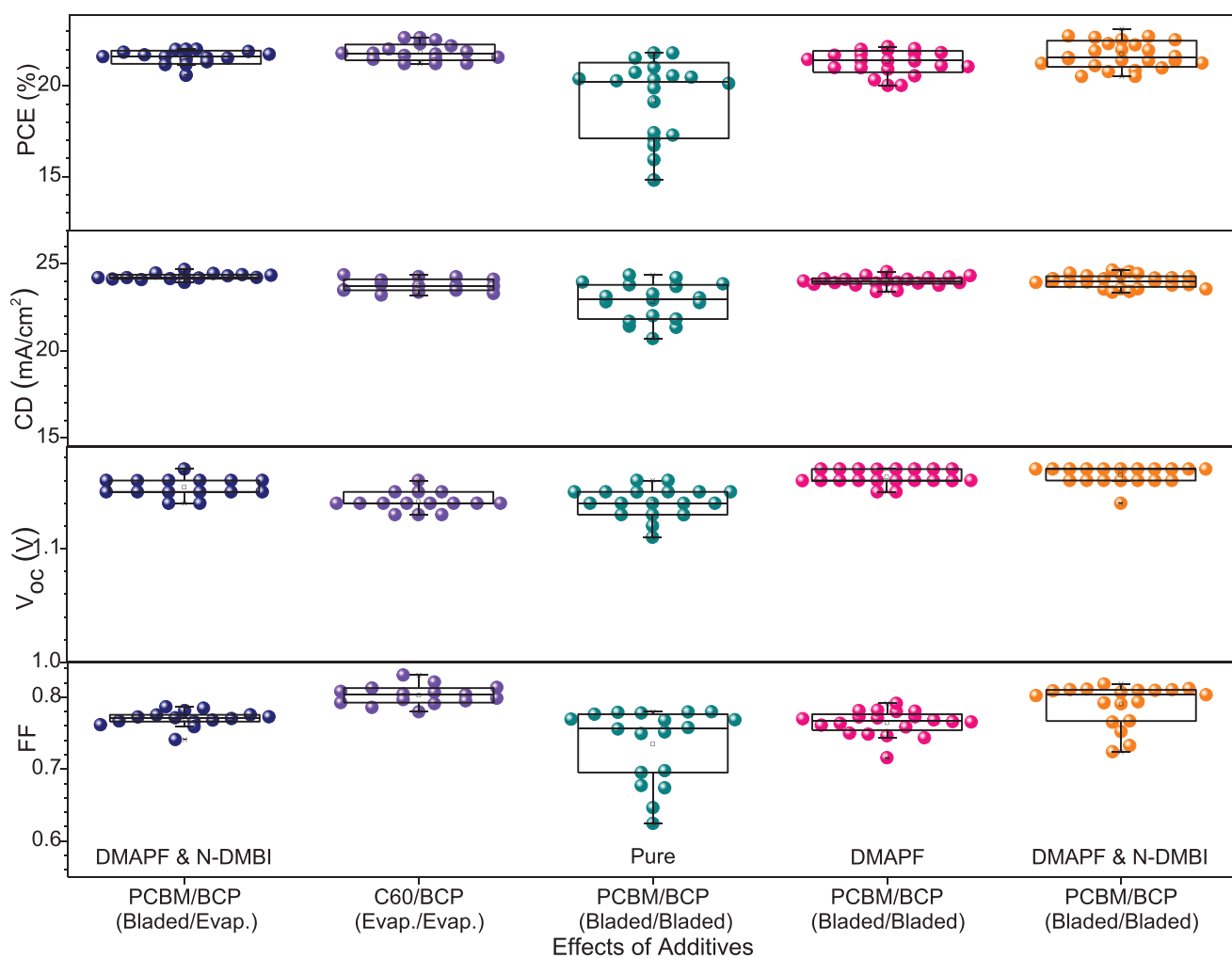

Figure 3. Device performance. Performance statistics of the devices (15–20 devices for each condition) fabricated with evaporated C$_{60}$, P-PCBM, and additives incorporated PCBM: J–V parameters from the devices measured from J_{sc} to V_{oc} under 1 sun illumination. Each dot represents a solar cell with active area of 0.08 cm^2.

ADVANCED
SCIENCE NEWS

www.advancedsciencenews.com

ADVANCED
MATERIALS

www.advmat.de

heterojunction on glass substrates using time-resolved photo-luminescence spectroscopy as shown in Figure S4 in the Supporting Information. It is observed that short decay time (τ_1 = 8.15 ns) of perovskite film without any ETL layer was significantly reduced to 2.22, 1.99, and 1.53 ns of PVSK/P-PCBM, PVSK/DMAPF-PCBM, and PVSK/N-DMBI-PCBM heterojunction, respectively. Short decay time (τ_1) was further reduced to 1.49 ns when both DMAPF and N-DMBI were introduced to PCBM, indicating better charge extraction capability of blade-coated A-PCBM layer than that of P-PCBM. To verify the doping capability of N-DMBI to PCBM, lateral conductivity of PCBM with and without N-DMBI were measured from a lateral architecture device using 4-point probe geometry with films coated on glass as shown in Figure S5 in the Supporting Information. It is found that N-DMBI increased the PCBM conductivity by 286 times.

To further test the capability of our formulated PCBM, devices with spin-coated A-PCBM on the same perovskite composition of $FA_{0.3}MA_{0.7}PbI_3$ and on a different composition of $Cs_{0.2}FA_{0.8}Sn_{0.5}Pb_{0.5}I_3$ (bandgap of ≈1.21 eV) were fabricated. Device performance statistics for both cases are shown in Figures S6 and S7 in the Supporting Information. The $FA_{0.3}MA_{0.7}PbI_3$ devices with evaporated and spin-coated ETL also showed comparable average efficiencies of 22.1 ± 0.6% from evaporated ETL and 22.1 ± 0.5% from A-PCBM, and the $Cs_{0.2}FA_{0.8}Sn_{0.5}Pb_{0.5}I_3$ narrow bandgap devices also showed comparable average efficiencies of 20.1 ± 0.2% from evaporated ETL and 20.2 ± 0.2% from A-PCBM. The results showed the A-PCBM can be broadly applied into perovskites of different compositions.

To further evaluate whether it is the $-N(CH_3)_2$ function group in DMAPF that mainly contributed to the enhance device performance, we chose three small molecules which have only partial function groups of DMAPF, as shown by the molecular structure in **Figure 4**a to replace DMAPF and evaluated the device efficiency. As shown in the Figure 4b,c & S8, DMAPF with both −Br and −NR$_2$ functional groups delivered a higher efficiency (21.6 ± 0.3%) than the other two derivatives (19.2 ± 2% for 2,7-dibromofluorene (DBF) and 19.7 ± 2% for 2,7-dibromo-9,9-di-n-octylfluorene (DOF), indicating −NR$_2$ functional groups played the critical role in forming conformal PCBM coating. In DOF, where $-N(CH_3)_2$ functional group is replaced by a long-chain −R group, the devices showed reproducible efficiency, but relatively lower short-circuit current density (J_{sc}), and open circuit voltage (V_{oc}), indicating long-chain −R group increasing insulating behavior and less effectively passivating the perovskite/PCBM interface due to the inability of −R group to bind the perovskite surface. On the other hand, DBF shows poorest device performance with relatively poor FF due to the absence of either −R or $-N(CH_3)_2$ indicating inability of DBF to disperse PCBM molecules in PCBM solution leading to incomplete coverage. Therefore, incomplete coverage of PCBM layer shows shunted devices with lower FF. We further tested other amine molecules with chemical structures shown in Figure 4d and Figure S9 (Supporting Information). All the molecules show similar solar cell performance, which confirmed the role of amine group is to disperse PCBM to form a conformal coating onto perovskite films.

3. Blading of BCP

After PCBM ink formulation, bathocuproine (BCP) ink was formulated and bladed onto PCBM layer to test the device performance. BCP is known as a common buffer (hole blocking)
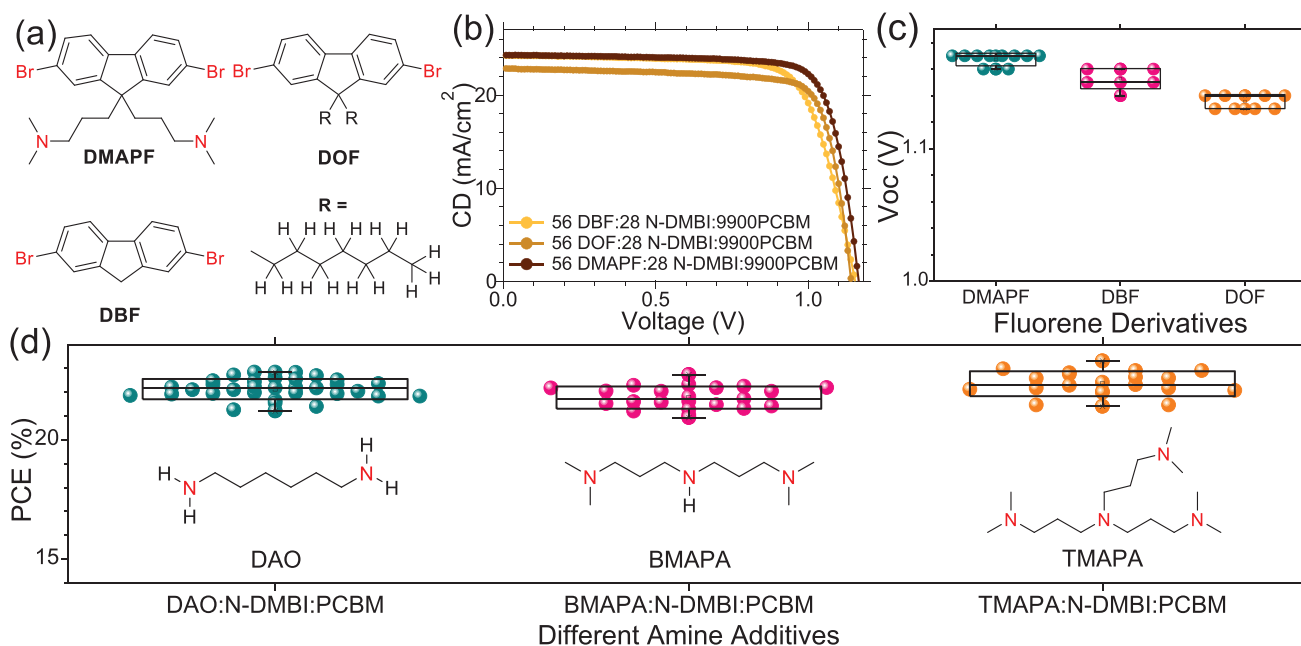

Figure 4. Roles of amine functional groups in device performance. a) Different fluorene derivatives, b,c) comparison of current density–voltage (*J–V*) curves and V_{oc} parameter of bladed-ETL devices (7–11 devices for each condition) fabricated with the different fluorene derivatives added in PCBM solutions, and d) comparison of device statistics of bladed-ETL devices (22–34 devices for each condition) with different amine-functionalized molecules incorporated in PCBM layers.
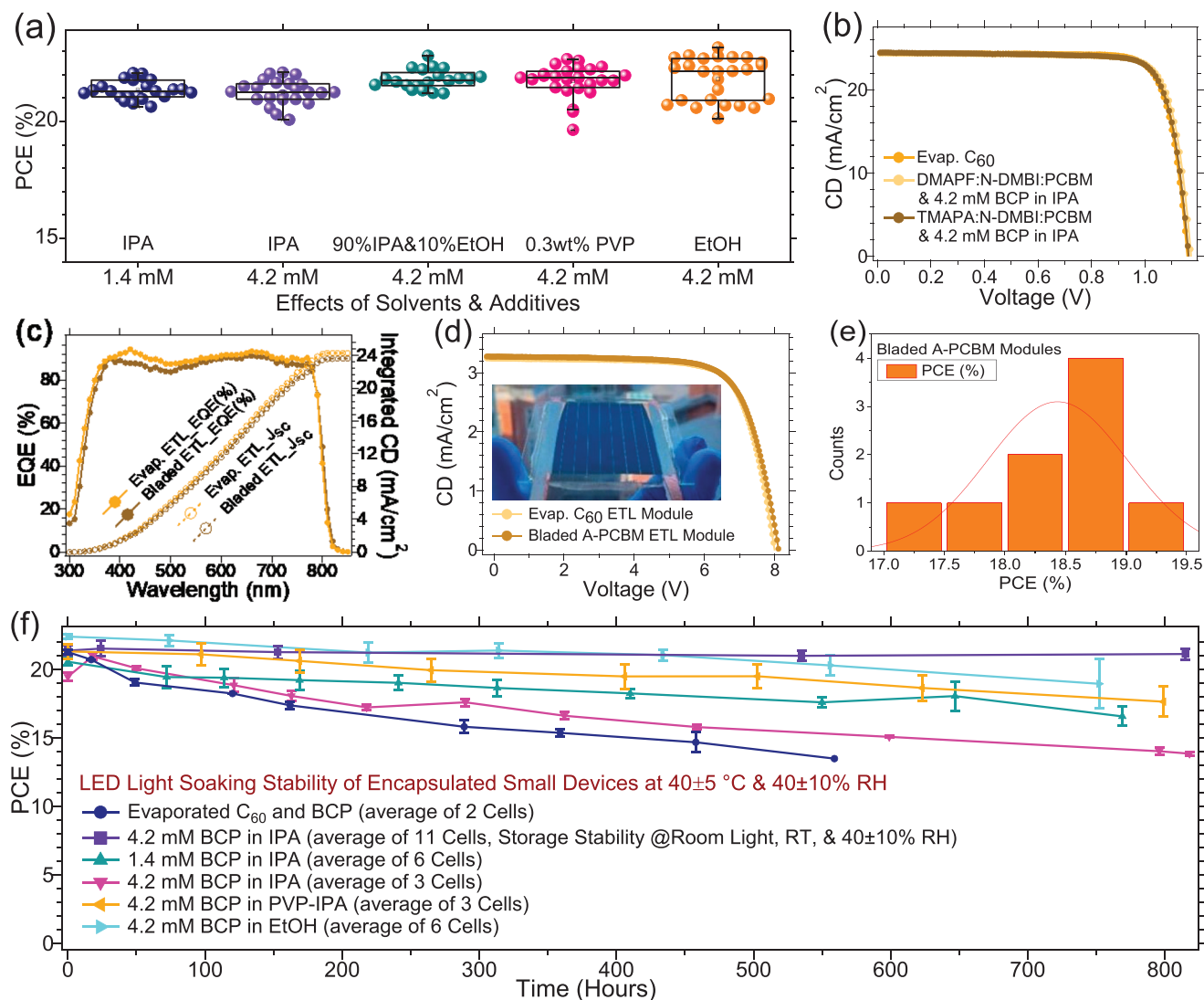
Figure 5. Stability of perovskite devices with bladed A-PCBM ETL and BCP. a) Performance statistics showing distribution of performance of devices (20–25 devices for each condition) fabricated with blade-coating of DMAPF and N-DMBI incorporated PCBM and BCP processed with different conditions, b,c) comparison of J–V characteristics and external quantum efficiency (EQE) spectra and integrated J_{sc} of thermally evaporated C_{60} and bladed A-PCBM small devices, d) comparison of J–V characteristics of thermally evaporated C_{60} and bladed A-PCBM modules, e) performance statistics of bladed A-PCBM modules (4–9 minimodules for each condition), and f) time-dependent stability of devices with DMAPF and N-DMBI incorporated PCBM and BCP processed with different conditions under light from a light-emitting diode (LED) at 40 ± 5 °C and 40 ± 10% RH.

layer between ETL and metal electrode in a p–i–n architecture device.[19] The device performance also greatly depends on BCP thickness and coverage, but bladed ink in commonly used solvent of IPA causes incomplete BCP coverage onto PCBM layer, making device performance irreproducible. This is caused by the too low solubility of BCP in IPA (0.5 mg mL^{-1}). We improved the quality of bladed BCP films using several different approaches: (i) using a solvent of ethanol (EtOH) which has much better solubility to BCP, and (ii) introducing additives such as poly(vinylpyrrolidone) (PVP) to improve dispersity of BCP molecules in solution. All the BCP solutions were bladed on A-PCBM layers to evaluate the device performance. **Figure 5**a and Figure S10 (Supporting Information) show performance statistics of all the bladed-ETL devices. It is clearly seen that devices with modified BCP ink were highly reproducible with enhanced average device efficiency. Devices with different

BCP solutions showed average efficiency of 21.3 ± 0.4% for 1.4×10^{-3} M BCP in IPA, 21.2 ± 0.5% for 4.2×10^{-3} M BCP in IPA, 21.8 ± 0.4% for 4.2×10^{-3} M BCP in EtOH-IPA, 21.7 ± 0.7% for 1.4×10^{-3} M BCP in PVP-IPA, and 21.7 ± 0.9% for 4.2×10^{-3} M BCP in EtOH. Figure 5b shows the typical J–V curves of devices with all-bladed ETL and evaporated ETL which almost overlap. The device with evaporated C_{60} and BCP delivered a PCE of ≈23.0% with a V_{OC} of 1.16 V, a J_{SC} of 24.30 mA cm^{-2}, and a FF of 0.815, whereas the bladed A-PCBM delivered a PCE of ≈23.1% with a V_{OC} of 1.17 V, a J_{SC} of 24.39 mA cm^{-2}, and a FF of 0.811. This shows the fully bladed ETL can replace the evaporated ones and still deliver the same device efficiency.

To verify current density of both evaporated C_{60} and bladed A-PCBM ETL small devices, EQE spectra were collected to calculate the current density. The integrated photocurrent of the EQE spectra of both evaporated and bladed-ETL devices reasonably

coincides with each other as shown in Figure 5c and values are calculated to be 24.1 and 23.6 mA cm^{-2} which are comparable to the average current density from J–V curve of solar cells. After ensuring reproducibility of small-area devices, we fabricated perovskite minimodules with both evaporated and bladed ETL with an aperture area of 25.03 cm^2 (7 sub cells with an aperture area of 3.575 cm^2 for each sub cell). Thirteen minimodules were fabricated, and all the minimodule performances are listed in Table S2 in the Supporting Information. From Figure 5d and Table S2 (Supporting Information), it is seen that minimodules with evaporated C$_{60}$ and bladed A-PCBM ETLs delivered an aperture efficiency of ≈19.3% (V_{OC} = ≈1.14 V; J_{SC} = 22.68 mA cm^{-2}; and FF = 0.746 for each sub cell) and 19.3% (V_{OC} = ≈1.16 V; J_{SC} = 22.96 mA cm^{-2}; FF = 0.723 for each sub cell), respectively, which verified the excellent uniformity of the all-bladed ETLs. The excellent ETL uniformity also leads to very good module reproducibility as indicated by the performance histogram of bladed-ETL minimodules shown in Figure 5e. Furthermore, the operational stability of both evaporated and bladed-ETL small solar cells with different conditions was also tested under 1 sun light at open circuit condition at 40 ± 5 °C and 40 ± 10% relative humidity (RH). The evaluation of efficiency with statistics are shown in Figure 5f and Figure S11 (Supporting Information). Devices with bladed ETL and BCP in EtOH retained 85% of its initial efficiency after 752 h of light soaking, while the devices with evaporated ETL lost 37% of their initial efficiency after 559 h of light soaking. We also tested the device stability under room light, which showed the bladed-ETL small devices retained 99% of initial efficiency after 815 h.

4. Conclusion

Additives incorporated solution-processed PCBM and BCP ink provided conformal ETL coating into perovskite layers. Thus, solar cells fabricated with modified PCBM and BCP inks showed an efficiency of over 23%, and minimodules with an area of 25.03 cm^2 showed an aperture efficiency of 19.3%, which are comparable to the best devices made with thermally evaporated C$_{60}$ and BCP. In addition, solar cells with blade-coated PCBM showed better light-soaking stability compared to that of thermally evaporated ETL devices by retaining over 85% of initial efficiency after 752 h of light soaking at 40 ± 5 °C and 40 ± 10% RH. Enhanced efficiency is attributed to the enhanced electrical conductivity of PCBM layer and conformal coating with close packing of PCBM with additives, whereas enhanced stability can be attributed to the better BCP coating. These results will accelerate the commercialization of perovskite solar cells via reducing cost and high throughput.

Conflict of Interest

The authors declare no conflict of interest.

Data Availability Statement

The data that support the findings of this study are available on request from the corresponding author. The data are not publicly available due to privacy or ethical restrictions.

[1] J. Jeong, M. Kim, J. Seo, H. Lu, P. Ahlawat, A. Mishra, Y. Yang, M. A. Hope, F. T. Eickemeyer, M. Kim, Y. J. Yoon, I. W. Choi, B. P. Darwich, S. J. Choi, Y. Jo, J. H. Lee, B. Walker, S. M. Zakeeruddin, L. Emsley, U. Rothlisberger, A. Hagfeldt, D. S. Kim, M. Grätzel, J. Y. Kim, *Nature* **2021**, *592*, 381.

[2] H. Min, D. Y. Lee, J. Kim, G. Kim, K. S. Lee, J. Kim, M. J. Paik, Y. K. Kim, K. S. Kim, M. G. Kim, T. J. Shin, S. Il Seok, *Nature* **2021**, *598*, 444.

[3] A. T. Mallajosyula, K. Fernando, S. Bhatt, A. Singh, B. W. Alphenaar, J. C. Blancon, W. Nie, G. Gupta, A. D. Mohite, *Appl. Mater. Today* **2016**, *3*, 96.

[4] Y. Deng, X. Zheng, Y. Bai, Q. Wang, J. Zhao, J. Huang, *Nat. Energy* **2018**, *3*, 560.

[5] J. Li, J. Dagar, O. Shargaieva, M. A. Flatken, H. Köbler, M. Fenske, C. Schultz, B. Stegemann, J. Just, D. M. Többens, A. Abate, R. Munir, E. Unger, *Adv. Energy Mater.* **2021**, *11*, 2003460.

[6] Q. Hu, L. Zhao, J. Wu, K. Gao, D. Luo, Y. Jiang, Z. Zhang, C. Zhu, E. Schaible, A. Hexemer, C. Wang, Y. Liu, W. Zhang, M. Grätzel, F. Liu, T. P. Russell, R. Zhu, Q. Gong, *Nat. Commun.* **2017**, *8*, 15688.

[7] D. N. Jeong, D. K. Lee, S. Seo, S. Y. Lim, Y. Zhang, H. Shin, H. Cheong, N. G. Park, *ACS Energy Lett.* **2019**, *4*, 1189.

[8] M. Jeong, I. W. Choi, K. Yim, S. Jeong, M. Kim, S. J. Choi, Y. Cho, J. H. An, H. B. Kim, Y. Jo, S. H. Kang, J. H. Bae, C. W. Lee, D. S. Kim, C. Yang, *Nat. Photonics* **2022**, *16*, 119.

[9] S. Chen, X. Xiao, H. Gu, J. Huang, *Sci. Adv.* **2021**, *7*, eabe8130.

[10] C. Liu, Y. Yang, K. Rakstys, A. Mahata, M. Franckevicius, E. Mosconi, R. Skackauskaite, B. Ding, K. G. Brooks, O. J. Usiobo, J. N. Audinot, H. Kanda, S. Driukas, G. Kavaliauskaite, V. Gulbinas, M. Dessimoz, V. Getautis, F. De Angelis, Y. Ding, S. Dai, P. J. Dyson, M. K. Nazeeruddin, *Nat. Commun.* **2021**, *12*, 6394.

[11] J. Li, X. Meng, Z. Huang, R. Dai, W. Sheng, C. Gong, L. Tan, Y. Chen, *Adv. Funct. Mater.* **2021**, *32*, 2105917.

[12] S. Castro-Hermosa, L. Wouk, I. S. Bicalho, L. de Queiroz Corrêa, B. de Jong, L. Cinà, T. M. Brown, D. Bagnis, *Nano Res.* **2021**, *14*, 1034.

[13] Y. Zheng, J. Kong, D. Huang, W. Shi, L. McMillon-Brown, H. E. Katz, J. Yu, A. D. Taylor, *Nanoscale* **2018**, *10*, 11342.

[14] D. K. Mohamad, J. Griffin, C. Bracher, A. T. Barrows, D. G. Lidzey, *Adv. Energy Mater.* **2016**, *6*, 1600994.

[15] D. Angmo, G. DeLuca, A. D. Scully, A. S. R. Chesman, A. Seeber, C. Zuo, D. Vak, U. Bach, M. Gao, *Cell Rep. Phys. Sci.* **2021**, *2*, 100293.

[16] J. Ciro, M. A. Mejía-Escobar, F. Jaramillo, *Sol. Energy* **2017**, *150*, 570.

[17] S. D. Stranks, S. D. Stranks, G. E. Eperon, G. Grancini, C. Menelaou, M. J. P. Alcocer, T. Leijtens, L. M. Herz, A. Petrozza, H. J. Snaith, *Science* **2013**, *342*, 341.

[18] G. Xing, N. Mathews, S. S. Lim, Y. M. Lam, S. Mhaisalkar, T. C. Sum, *Science* **2013**, *6960*, 498.

[19] J. Y. Jeng, Y. F. Chiang, M. H. Lee, S. R. Peng, T. F. Guo, P. Chen, T. C. Wen, *Adv. Mater.* **2013**, *25*, 3727.

[20] A. Kojima, K. Teshima, Y. Shirai, T. Miyasaka, *J. Am. Chem. Soc.* **2009**, *131*, 6050.

[21] M. M. Lee, J. Teuscher, T. Miyasaka, T. N. Murakami, H. J. Snaith, *Science* **2012**, *338*, 643.

[22] Q. Jiang, Z. Chu, P. Wang, X. Yang, H. Liu, Y. Wang, Z. Yin, J. Wu, X. Zhang, J. You, *Adv. Mater.* **2017**, *29*, 1703852.

[23] Y. Sun, J. H. Seo, C. J. Takacs, J. Seifter, A. J. Heeger, *Adv. Mater.* **2011**, *23*, 1679.

[24] D. Liu, T. L. Kelly, *Nat. Photonics* **2014**, *8*, 133.

[25] C. I. Wang, C. C. Hua, *J. Phys. Chem. B* **2015**, *119*, 14496.

[26] S. Chen, X. Dai, S. Xu, H. Jiao, L. Zhao, J. Huang, *Science* **2021**, *373*, 902.

[27] C.-Q. Sheng, W.-J. Li, Y.-Y. Du, G.-H. Chen, Z. Chen, H.-Y. Li, H.-N. Li, *AIP Adv.* **2015**, *5*, 097201.